Wave Motion 128 (2024) 103324

Contents lists available at ScienceDirect

Wave Motion

journal homepage: www.elsevier.com/locate/wamot

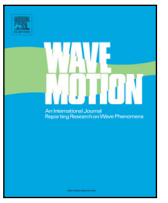

Existence, stability and spatio-temporal dynamics of time-quasiperiodic solutions on a finite background in discrete nonlinear Schrödinger models

E.G. Charalampidis [a], G. James [b], J. Cuevas-Maraver [c,d,*], D. Hennig [e], N.I. Karachalios [e], P.G. Kevrekidis [f]

[a] Mathematics Department, California Polytechnic State University, San Luis Obispo, CA 93407-0403, USA
[b] Univ. Grenoble Alpes, CNRS, Inria, Grenoble INP, LJK, 38000 Grenoble, France
[c] Grupo de Física No Lineal, Departamento de Física Aplicada I, Universidad de Sevilla, Escuela Politécnica Superior, C/ Virgen de África, 7, 41011 Sevilla, Spain
[d] Instituto de Matemáticas de la Universidad de Sevilla (IMUS), Edificio Celestino Mutis, Avda. Reina Mercedes s/n, 41012 Sevilla, Spain
[e] Department of Mathematics, University of Thessaly, Lamia 35100, Greece
[f] Department of Mathematics and Statistics, University of Massachusetts Amherst, Amherst, MA 01003-4515, USA

ARTICLE INFO

Keywords:
Discrete nonlinear Schrödinger equation
Solitons
Breathers
Discrete solitons
Quasi-periodic solitons
Rogue waves

ABSTRACT

In the present work we explore the potential of models of the discrete nonlinear Schrödinger (DNLS) type to support spatially localized and temporally quasiperiodic solutions on top of a finite background. Such solutions are rigorously shown to exist in the vicinity of the anti-continuum, vanishing-coupling limit of the model. We then use numerical continuation to illustrate their persistence for finite coupling, as well as to explore their spectral stability. We obtain an intricate bifurcation diagram showing a progression of such solutions from simpler ones bearing single- and two-site excitations to more complex, multi-site ones with a direct connection of the branches of the self-focusing and self-defocusing nonlinear regime. We further probe the variation of the solutions obtained towards the limit of vanishing frequency for both signs of the nonlinearity. Our analysis is complemented by exploring the dynamics of the solutions via direct numerical simulations.

1. Introduction

The topic of nonlinear dynamical lattices and their localized modes has received considerable attention over the past 4 decades, especially since the illustration of their generic emergence in anharmonic crystals [1], and also the rigorous mathematical proof of their existence under suitable non-resonance conditions [2]. Indeed, relevant progress has been by now summarized in a number of influential reviews such as [3,4]. Importantly, beyond the mathematical and computational analyses of the existence of such modes, a key reason for their extensive study has, arguably, been the impact of associated prototypical models in advancing our understanding as concerns light propagation in optical waveguides [5] and mean-field models of atomic condensates in optical lattices [6]. In both of these central applications, a prototypical dynamical model that has contributed to the analysis, simulations and experimental progress has been the discrete nonlinear Schrödinger (DNLS) equation [7]. In addition to its time-honored history, the DNLS is a model that continues to lead to new experiments and corresponding insights, as, e.g., in the recent work of [8,9]; see also the review of [10].

* Corresponding author.
E-mail address: jcuevas@us.es (J. Cuevas-Maraver).

https://doi.org/10.1016/j.wavemoti.2024.103324
Received 11 February 2024; Accepted 17 March 2024
Available online 24 March 2024

On the other hand, a topic of ever growing interest over the last (especially) 15 years has been the dynamics of rogue or freak waves [11]. While observations of such have existed for over half a century [12] and the well-known measurement of the Draupner wave on the first day of 1995 has captured the attention of the physics, engineering and mathematics communities alike, it has been mostly over the last decade and a half that numerous relevant developments have arisen especially on the nonlinear analysis of such waves, as motivated by carefully-controlled experiments. Indeed, the leveraging of novel detection techniques to observe them in optical systems [13,14] has led to numerous further explorations within that field [15–18]. In parallel, the ability to produce fluid experiments of fundamental and higher-order rogue waves emerged in the works of [19–21], and led to the re-creation of the Draupner wave in [22]. In addition to the broader relevance of these ideas as argued, e.g., in other fields such as plasmas [23], and very recently superfluids [24], the maturation of these efforts can be recognized in a number of impactful reviews such as [25–29]. The experimental techniques and observations of such waves continue to improve in areas such as nonlinear optics, as evidenced by numerous recent remarkable experiments such as [30,31].

Our original aim in the present work was to explore the potential inter-connection between these important current research themes. Indeed, this has been an ongoing effort that has identified analogues of rogue-type structures (such as the famous Peregrine (P) soliton [32], the Kuznetsov-Ma (KM) soliton [33,34] or the Akhmediev breather (AB) [35]) in the integrable discrete realm of the so-called Ablowitz–Ladik (AL) model [36]. More recent efforts from a subset of the present authors have attempted to leverage the so-called Salerno model [37] to homotopically interpolate between the AL and the physically realistic DNLS model [38,39]. However, the relevant computational continuation efforts at the bifurcation level typically encountered turning points, leading them to discover unprecedented AL solutions [39] bearing an oscillatory background, without necessarily improving our understanding of the DNLS (or the continuum, for that matter) limit. Motivated by this finding, we raise the question of whether such periodic solutions can be identified in DNLS-type models that sit on top of a finite, i.e., flat background. It is important to highlight here that leveraging the phase invariance of the DNLS model and factoring out a constant background, one can seek time-periodic waveforms which are *quasiperiodic* ones in the original model, in a way reminiscent of the works of [40,41] which, however, sought such solutions on top of a vanishing background or of a stationary soliton, respectively.

Motivated by the above observations, we start from the highly-controllable anti-continuum (AC) limit of vanishing coupling across the lattice nodes. We show that in the neighborhood of such a limit, breathing-in-time solutions (in the frame "co-rotating" with a certain frequency, hence quasiperiodic in the original frame) *rigorously* exist. We then corroborate these findings through numerical computations that reveal an intricate bifurcation structure connecting such breathing states between the focusing and the defocusing DNLS settings. Although our dynamical simulations reveal the nature of the solutions we identified, it is important to distinguish their characteristics from the inherent features of rogue waves. The latter include high-amplitude waveforms that "appear out of nowhere and disappear without a trace", while exceeding a certain amplitude threshold [42]. Instead, our waveforms will be weakly quasiperiodically breathing on top of a fixed density profile. Regardless, the obtained waveforms, while only motivated by the rogue patterns, constitute a novel class of quasiperiodic solutions of the experimentally relevant DNLS equation and as such are of potential interest, including in experiments within nonlinear optics (optical waveguides) [5] and atomic physics (Bose–Einstein condensates in optical lattices) [6]. Our presentation is structured as follows. In Section 2, we present the rigorous proof of existence of the states of interest, while in Section 3, we detail our numerical continuation, spectral stability and nonlinear dynamics results. Finally, in Section 4, we summarize our findings and present our conclusions.

2. Rigorous analysis of time-quasiperiodic solutions to DNLS models

We consider the general model

$$i\,\dot{\psi}_n + \psi_n\, f(|\psi_n|^2) + \sum_{p\in\mathbb{Z}} K_{n-p}\,\psi_p = 0, \quad n\in\mathbb{Z}, \tag{1}$$

where $f\in C^1((0,\infty),\mathbb{R})$. We denote by $\ell_1(\mathbb{Z},\mathbb{K})$ the classical Banach space of summable sequences in $\mathbb{K}=\mathbb{R}$ or $\mathbb{C}$. We assume that the sequence $K=(K_n)_{n\in\mathbb{Z}}\in\ell_1(\mathbb{Z},\mathbb{R})$ satisfies $\sum_{n\in\mathbb{Z}} K_n = 0$, and denote the closed linear subspace of $\ell_1(\mathbb{Z},\mathbb{R})$ consisting of zero-sum sequences by S_0. This class of models encompasses the generalized form of the DNLS equation [7] corresponding to $K_0=-2d$, $K_{\pm1}=d$ and $K_n=0$ elsewhere, with d being a coupling parameter.

With the zero-sum assumption on the sequence K, Eq. (1) admits time-periodic solutions of the form

$$\psi_n(t) = R\,e^{i\,(\Omega\,t+\varphi)}, \tag{2}$$

with nonvanishing amplitude $R>0$, frequency $\Omega=f(R^2)$ and phase shift φ. In what follows, we consider a solution of the form (2) with $\varphi=0$ and assume that the nondegeneracy condition $f'(R^2)\neq 0$ is satisfied. This holds still, in particular, for the classical cubic nonlinearities, where f' is a nonvanishing constant.

We look for breather solutions of Eq. (1) on a background, corresponding to spatially localized perturbations of solution (2), quasiperiodic in time with two fundamental frequencies. For this purpose, we set

$$\psi_n(t) = e^{i\,\Omega\,t}\,u_n(t), \tag{3}$$

with u_n being time-periodic with frequency $\omega_b = f(A^2)-\Omega$, and for some fixed $A>0$. Substitution in Eq. (1) yields

$$i\,\dot{u}_n + u_n\,[\,f(|u_n|^2)-\Omega\,] + \sum_{p\in\mathbb{Z}} K_{n-p}\,u_p = 0, \quad n\in\mathbb{Z}. \tag{4}$$

We assume $f'(A^2) \neq 0$, and the nonresonance condition $f(A^2) \neq \Omega$, i.e., $\omega_b \neq 0$ (so that there are two distinct frequencies in the solution (3)). In addition, we consider time-reversible solutions satisfying $u_n(-t) = \bar{u}_n(t)$, where the notation $\bar{u}_n$ is used for complex conjugate.

In the anti-continuum (AC) limit $K = 0$ [2], the system given by Eq. (4) becomes uncoupled, and admits solutions u_n^0 taking the form

$$u_n^0(t) = \begin{cases} A\, e^{i\,\omega_b t} & \text{if } \ n \in \mathbb{I}^+, \\ -A\, e^{i\,\omega_b t} & \text{if } \ n \in \mathbb{I}^-, \\ R & \text{if } \ n \in \mathbb{I}, \end{cases} \tag{5}$$

where $\mathbb{I}^+$, $\mathbb{I}^-$ are arbitrary finite subsets of $\mathbb{Z} = \mathbb{I} \cup \mathbb{I}^+ \cup \mathbb{I}^-$. In the sequel, we search for solutions $u = (u_n(.))_{n\in\mathbb{Z}}$ of Eq. (4) close to the form (5) when K is small in $\ell_1(\mathbb{Z})$. For this purpose, we use the ansatz

$$u_n = u_n^0 + y_n, \tag{6}$$

where the perturbation $y = (y_n(.))_{n\in\mathbb{Z}}$ is sought in a spatially localized and time-periodic form with period $T = 2\pi/\omega_b$. More precisely, we define, for all $m \geq 0$, the Banach space

$$X_m = \left\{ y \in C^m\big(\mathbb{R}/T\mathbb{Z}, \ell_1(\mathbb{Z},\mathbb{C})\big),\ y_n(-t) = \bar{y}_n(t) \right\}.$$

(X_m is endowed with the usual C^m norm) and we assume $y \in X_1$. We substitute expression (6) in Eq. (4) and obtain the following equation for the perturbation y:

$$0 = i\,\dot{y}_n + u_n^0 \left(f(|u_n^0 + y_n|^2) - f(|u_n^0|^2) \right) + y_n \left(f(|u_n^0 + y_n|^2) - \Omega \right) + \sum_{p\in\mathbb{Z}} K_{n-p}\,(u_p^0 + y_p), \quad n \in \mathbb{Z}. \tag{7}$$

Let us identify y with $\tilde{y} = (\mathrm{Re}(y), \mathrm{Im}(y)) \in \tilde{X}_1$, where for all $m \geq 0$

$$\tilde{X}_m = \left\{ (a_n(.), b_n(.))_{n\in\mathbb{Z}} \in C^m\big(\mathbb{R}/T\mathbb{Z}, \ell_1(\mathbb{Z},\mathbb{R})^2\big), a_n(-t) = a_n(t),\ b_n(-t) = -b_n(t) \right\}.$$

System (7) can be considered as a nonlinear equation $F(\tilde{y}, K) = 0$ with $F \in C^1(\tilde{X}_1 \times S_0, \tilde{X}_0)$ defined by the right-hand-side of Eq. (7) with $F(0,0) = 0$.

In order to solve Eq. (7) for $K \approx 0$ using the implicit function theorem, we need to check the invertibility of $L = D_{\tilde{y}} F(0,0) \in \mathcal{L}(\tilde{X}_1, \tilde{X}_0)$ (the $\mathcal{L}$ stands for bounded linear operator). Let $\tilde{f} = (a_n(.), b_n(.))_{n\in\mathbb{Z}} \in \tilde{X}_0$ and search for $\tilde{y} \in \tilde{X}_1$ such that $L\,\tilde{y} = \tilde{f}$. This problem can be rewritten as

$$f_n = \begin{cases} i\,\dot{y}_n + R^2 f'(R^2)\,(y_n + \bar{y}_n), & n \in \mathbb{I}, \\ i\,\dot{y}_n + A^2 f'(A^2)\,(y_n + e^{2i\,\omega_b t}\,\bar{y}_n) + \omega_b y_n, & n \in \mathbb{Z}\setminus\mathbb{I}, \end{cases} \tag{8}$$

with $f_n = a_n + i\,b_n$, $f_n(-t) = \bar{f}_n(t)$. We start by solving the above equations for any given $n \in \mathbb{I}$. Expanding y_n, f_n in Fourier series (omitting the index n in the Fourier coefficients for notational simplicity), we have

$$y_n(t) = \sum_{k\in\mathbb{Z}} c_k\, e^{ik\omega_b t}, \qquad f_n(t) = \sum_{k\in\mathbb{Z}} b_k\, e^{ik\omega_b t},$$

with $c_k, b_k \in \mathbb{R}$ due to time-reversibility symmetry. Substitution of the above expansions in Eq. (8) yields

$$c_0 = b_0/(2R^2 f'(R^2)), \tag{9a}$$

$$c_k = \frac{R^2 f'(R^2)}{k^2\omega_b^2}(b_{-k} - b_k) - \frac{b_k}{k\omega_b}, \tag{9b}$$

for all $k \neq 0$. Similarly, for $n \in \mathbb{Z}\setminus\mathbb{I}$ we obtain

$$c_1 = b_1/(2A^2 f'(A^2)), \tag{10a}$$

$$c_k = \frac{A^2 f'(A^2)}{(k-1)^2\omega_b^2}(b_{2-k} - b_k) - \frac{b_k}{(k-1)\omega_b}, \tag{10b}$$

for all $k \neq 1$. This yields a unique solution $y \in X_1$ to Eq. (8), where C^1-regularity follows from a standard bootstrap argument. As a result, the linearized map L is invertible.

Consequently, by the implicit function theorem, the solution $y = 0$ to Eq. (7) with $K = 0$ can be continued for $K \approx 0$ into a unique solution $y = Y(K) \in X_1$, where Y is a C^1 map defined on a neighborhood of $K = 0$ in S_0 and $Y(0) = 0$. Equivalently, for all $K \approx 0$ in S_0, Eq. (4) admits a unique T-periodic reversible solution such that $\|u - u^0\|_{X_1}$ is small, which depends smoothly on K.

We conclude this analysis by briefly mentioning some symmetry considerations when $K_{-n} = K_n$ (as in the generalized DNLS equation), a case when Eq. (4) has the invariance $n \to -n$. If the solution u^0 in the AC limit is site-centered, i.e. $u_{-n}^0(t) = u_n^0(t)$, then by uniqueness of the local continuation u one has also $u_{-n}(t) = u_n(t)$. This case occurs in particular for $u_0^0(t) = \pm A\, e^{i\omega_b t}$ and $u_n^0(t) = R$ elsewhere. Similarly, if u_0 is bond-centered, i.e. $u_n^0(t) = u_{1-n}^0(t)$, then the local continuation $u_n(t)$ has the same symmetry. This is the case in particular if $u_0^0(t) = u_1^0(t) = \pm A\, e^{i\omega_b t}$ and $u_n^0(t) = R$ elsewhere.

3. Numerical computations

Our analysis so far, has been kept quite general to illustrate the breadth of the relevant ideas. However, motivated by the experimental realizability of the nearest-neighbor, cubic DNLS model [5,6], in the numerical computations that follow, we restrict our considerations to this model, which corresponds to the cases $f(|u_n|^2) = |u_n|^2$ and $K_{n-p} = d\delta_{n-p,\pm 1} - 2d\delta_{n-p,0}$ (where the Kronecker-δ is implied). This way, Eq. (4) reduces to:

$$i\dot{u}_n + d\left(u_{n+1} - 2u_n + u_{n-1}\right) + \left(|u_n|^2 - \Omega\right) u_n = 0. \tag{11}$$

In the numerical computations discussed in this section, we identify time-periodic solutions $u_n(t) = u_n(t+T)$ with period $T = 2\pi/\omega_b$ (or, equivalently with frequency ω_b) to Eq. (11). We carry out our computations on a lattice with $N = 50$ sites where periodic boundary conditions are imposed, i.e., $u_{-N/2} = u_{N/2}$. In our visualization of the relevant waveform, we normalize its background density (i.e., square modulus equal to Ω which is set to 1 hereafter, i.e., $\Omega \equiv 1$). Similarly to [39], time-periodic solutions (on top of the background frequency Ω) are sought by using the ansatz:

$$u_n(t) = 1 + \sum_{k=-\infty}^{\infty} \mathcal{U}_{n,k} e^{ik\omega_b t}. \tag{12}$$

Upon substituting this to the DNLS Eq. (11) leads to a root-finding problem for the Fourier coefficients $\mathcal{U}_{n,k}$ that is solved by means of Newton's method. We note that we truncated the series [cf. Eq. (12)] by fixing $|k| \leq m$ with $m = 21$, hence considering $2m+1 = 43$ Fourier modes in time. Those were proven to be enough to resolve the $1 + 0i$ Floquet multiplier associated with the linearization of the DNLS around the solution, a mode that is theoretically expected to be present due to the Hamiltonian nature of the model. Upon convergence in Newton's method, we reconstruct the solution u_n at $t = 0$ by summing over the Fourier modes according to Eq. (12), and then using the resulting $u_n(t)$ in Eq. (3). We explore the configuration space of time-periodic solutions to the DNLS equation by performing a pseudo-arclength continuation [43] over the coupling parameter d and frequency ω_b. At each continuation step, a Floquet stability analysis is carried out through the solution of the variational equations for the associated monodromy matrix, in order to determine the stability characteristics of the solutions we found; see [39] for further details about the setup of the stability problem.

In Fig. 1, we summarize our numerical results for site- and bond-centered time-periodic solutions that our solvers converged to. In particular, we show branches of time-periodic solutions with $\omega_b = 8$ and background unit amplitude where the set $\mathbb{I}^-$ consists of a single (top panel) and double (bottom panel) site near the AC limit (and $\mathbb{I}^+$ is empty), analogously to the well-known site-centered and bond-centered solutions (on top of a vanishing background) of the DNLS model [7]. As a relevant bifurcation diagnostic, we measure the average norm of the solutions $\langle N \rangle = \sum_n \sum_{k=-m}^{m} |\mathcal{U}_{n,k}|^2$, and depict the densities $|u_n|^2$ of the solutions' spatial profile (through its reconstruction from Eq. (12)) and their Floquet spectra in Fig. 1.

Let us begin our discussion by going through the results on site-centered breathers as they are summarized in the top panel of Fig. 1. It can be discerned from the figure that a state of this type at the AC limit can be continued over the coupling strength d, see, Fig. 1(a), and up to $d \approx 0.4$ before encountering a turning point that leads to a branch with practically a central and a number of lateral excited sites as this is shown in Fig. 1(b). The relevant continuation goes through $d = 0$ over to the defocusing nonlinearity setting of $d < 0$ (discussed in more detail next), and then coming back to the focusing regime again with states involving more intense lateral excitations as these are progressively shown in Figs. 1(c) and (d). It is interesting to observe that every second one of these branches features a node that is nearly of vanishing amplitude; note that a similar feature is present in the panels (e)–(h) of the defocusing problem below. All 4 of these sets of panels are for the same coupling of $d = 0.2$. The same sequence of defocusing and focusing segments continues for multiple additional turning points (the remaining ones of which occur around $d \approx 0.35$).

In a similar vein, but now for $d = -0.1$, the top panel of Fig. 1 also shows four examples of the branches of (site-centered) time-periodic waveforms for the case of a defocusing nonlinearity, see the panels (e)–(h) therein. Indeed, we observe a similar pattern as one moves through the different portions of the relevant branches and the associated turning points (compare the panels (e) and (f) with (b) and (a), respectively, of the focusing regime). Gradually more nodes deviate from the background amplitude, forming a progressively more delocalized breathing excitation as is shown in panels (g) and (h) therein. Here, though, contrary to the focusing case where the additional excitations are higher than the background, the additional excited sites have densities below those of the background. Furthermore, it is relevant to also make some additional observations. Firstly, we remark that each pair of focusing branches in the diagram segues into a pair (again involving a turning point) of defocusing branches, then on to another focusing loop and so on. Yet, it is interesting to also examine how the change of stability of the relevant waveforms occurs along this continuation, as shown in the bottom of each panel in Fig. 1, with the latter representing the corresponding Floquet multipliers of the monodromy matrix.

For the focusing portions, the branch is modulationally unstable, in line with the earlier associated calculation of [44] (see also [39]), as is reflected in the real Floquet multipliers of the associated linearization around the periodic orbit; see Figs. 1(a)–(d). Yet, as the AC limit of $d = 0$ is approached, the modulational instability (MI) band shrinks and subsequently the relevant multipliers reside on the unit circle for the defocusing case of $d < 0$, as shown in Figs. 1(e)–(h). Nevertheless, it is interesting to highlight that the (site-centered) breathing waveforms for the case of Fig. 1(e) (and more generally in the $d < 0$ branches) are very weakly unstable due to *isolated* unstable pairs of real multipliers. The number of pairs increases by one for every higher branch considered (two in Fig. 1(f), three in Fig. 1(g), four in Fig. 1(h), etc. within Fig. 1).

We briefly highlight the numerical results for bond-centered breathers as they are shown in the bottom panel of Fig. 1. Upon analytically constructing the relevant state from the AC limit, see Fig. 1(i), the bifurcation diagram reveals similar features of the

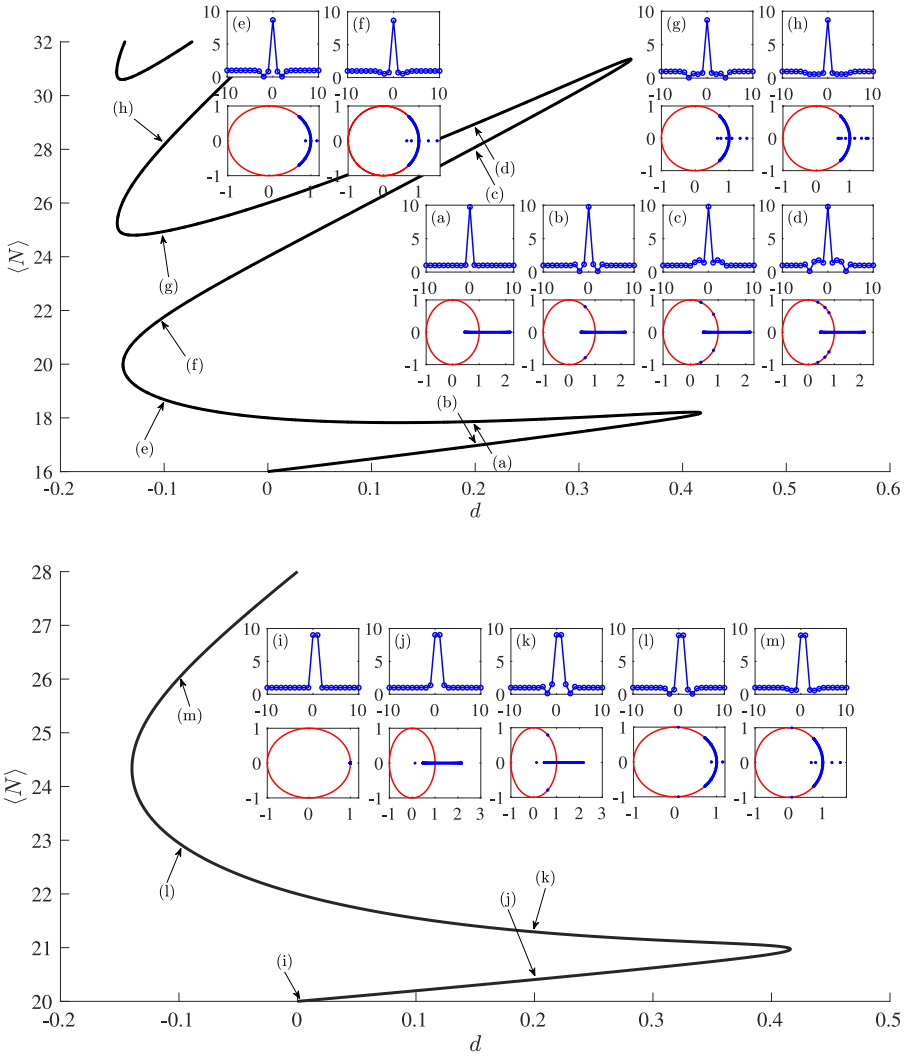

Fig. 1. Bifurcation diagrams (showcasing the dependence of the average norm of the solutions $\langle N \rangle$ vs the coupling constant d) and associated solutions as well as their Floquet spectra for site- (top panel) and bond-centered (bottom panel) time-periodic solutions to the DNLS with $\omega_b = 8$ and $\Omega = 1$. The insets in both panels showcase the density, i.e., the modulus square $|u_n|^2$ of the solutions found together with their spectra. The labels therein are associated with the arrows in the respective bifurcation diagrams (see text for details). For the site-centered breathers, the panels (a)–(d) depict 4 examples of solutions in the focusing problem whereas the panels (e)–(h) showcase 4 such in the defocusing problem. In the bond-centered case, in addition to the AC limit profile (i), we demonstrate 2 examples in each of the focusing (see (j) and (k)) and defocusing (see (l) and (m)) regimes. (For interpretation of the references to color in this figure legend, the reader is referred to the web version of this article.)

states presented herein with the site-centered ones as regards their background structure and stability characteristics (compare the site-centered states shown in the top panel of the figure with the bond-centered ones of the bottom panel, respectively). Also, we notice that the bond-centered breathers are similarly modulationally unstable in the focusing regime although they become only weakly unstable in the defocusing regime similarly to their site-centered counterparts. Again, we highlight that the instability in the defocusing regime is due to the existence of an isolated unstable pair of real multipliers (see, Fig. 1(l)), and the number of the unstable pairs increases by one as we move to higher branches, see, indicatively, Fig. 1(m). It is interesting to observe that the lowest defocusing bond-centered branch (l) in the bottom panel of Fig. 1 has the same number of unstable eigendirections as the site-centered branch of the defocusing problem in panel (e) of the top part of Fig. 1.

Subsequently, we were interested in exploring the approach of the relevant branches of site-centered solutions towards the limit where the frequency ω_b of the time-periodic solution approaches 0. While the patterns obtained are not rogue waves, the latter limiting process for rogue waves holds particular interest as it turns the so-called KM solutions into the limiting Peregrine solitonic structure. To explore this in Fig. 2, we performed a continuation both for the focusing case (top panel) and for the defocusing one (bottom panel) towards the vanishing frequency limit, indeed for different values of the coupling constant d. Naturally, for none of the cases, were we able to reach the limit (as the solution loses its periodic orbit character). Yet, it was interesting to observe that

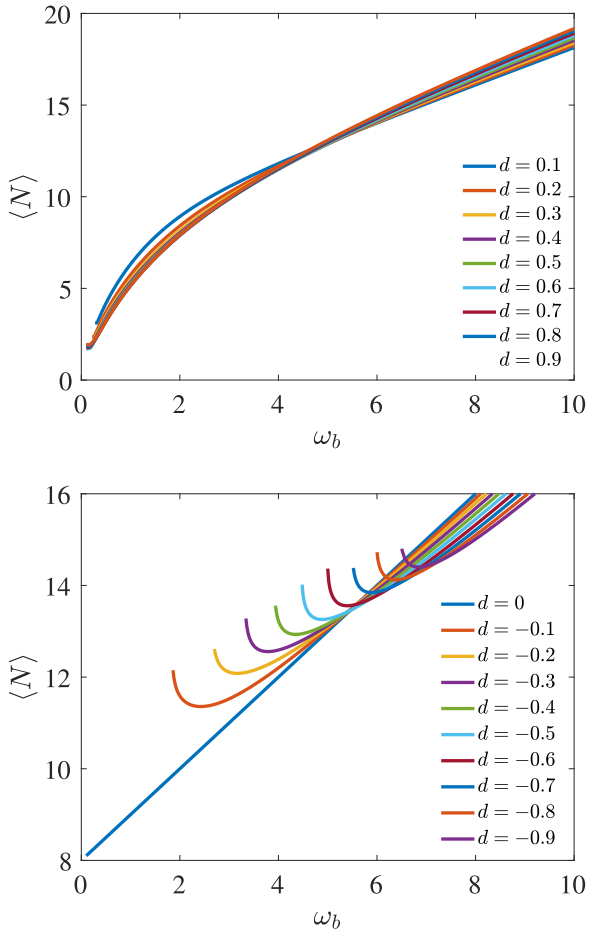

Fig. 2. The average power (sum of the square intensities of the Fourier coefficients) of the solution as a function of the frequency ω_b for the focusing case (top panel) and the defocusing one (bottom panel). Different values of the coupling constant d are illustrated by the different curves, according to the legend. (For interpretation of the references to color in this figure legend, the reader is referred to the web version of this article.)

while the focusing branches could be continued in a concave down form towards this limit in the (average) "power" dependence (the sum of the square intensities of the Fourier coefficients) vs. the frequency ω_b, this was not the case in the defocusing setting. In the latter, a turning point always appeared which is also tantamount to a stability change, in line with the classic criterion of [45]. The relevant defocusing model turning point occurred closer to frequencies $\omega_b \to 0$, the smaller (in absolute value) the coupling strength d was.

Finally, we move to the results on the spatio-temporal evolution of the quasiperiodic (in the original frame — time-periodic in their modulus evolution) solutions presented in Figs. 3 and 4 (again, with $\omega_b = 8$ and $\Omega = 1$) both for the focusing and defocusing cases. We only considered site-centered breathers since the results for bond-centered ones are similar and are omitted herein. The panels (a)–(d) in Fig. 3 showcase the spatio-temporal evolution of the amplitude $|u_n|$ of (site-centered) breathers which respectively connect with the labels (a) and (d) (focusing regime) as well as (f) and (h) (defocusing regime) of the top panel of Fig. 1. We note in passing that we depict the amplitude and not the density, i.e., $|u_n|^2$ of the solutions therein due to the dim variation of the profiles over a period. We used the breather that our Newton solver converged to as an initial condition, and integrated Eq. (11) forward in time. The terminal times for the results shown in panels (a), (b), and (d) are $60\,T$, and $120\,T$ for (c).

It can be discerned from these panels that all solutions are dynamically unstable although the ones shown in panels (a) and (b) (being examples of the focusing regime) are modulationally unstable per our Floquet stability analysis (see, their Floquet spectra in (a) and (f) in the top panel of Fig. 1). Around $t \approx 33$ and $t \approx 35$ in Figs. 3(a) and (b), the instability of the background (due to MI) manifests itself and appears to also partially affect the core structure of the solution. The center of the solution, i.e., at $n = 0$ remains chiefly unaltered even up to $t = 1000\,T$ although the remaining nodes that were originally deviated from the background are more drastically modified (results not shown). On the contrary, in Figs. 3(c) and (d), i.e., defocusing regime, the instability is emanating now from the core structure of the solution (i.e., from the point spectrum instability of the state, while the background is in this case modulationally stable), see the Floquet spectra in (f) and (h) in the top panel of Fig. 1. Interestingly, however, and somewhat similarly to the panels (a) and (b) in the figure, the solutions at $n = 0$ in panels (c) and (d) remain robust and mostly unaltered in

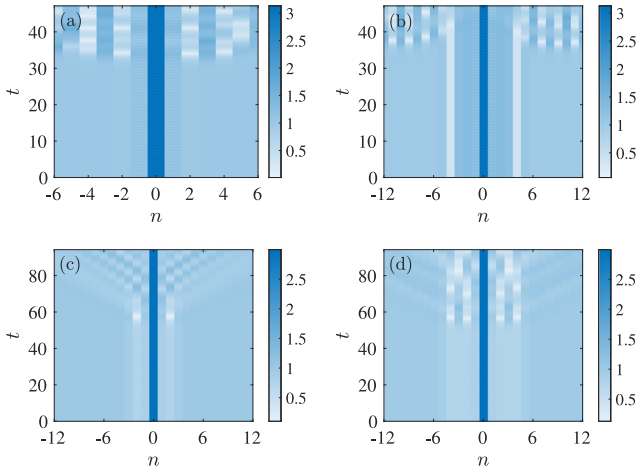

Fig. 3. Spatio-temporal evolution of the amplitude $|u_n|$ of the quasiperiodic solutions to the DNLS associated with the top panel of Fig. 1 with $\omega_b = 8$ (see also Fig. 4). The labels (a)–(d) herein connect with the solutions of Fig. 1 labeled with (a) ($d = 0.2$), (d) ($d = 0.2$), (f) ($d = -0.1$), and (h) ($d = -0.1$), respectively. (For interpretation of the references to color in this figure legend, the reader is referred to the web version of this article.)

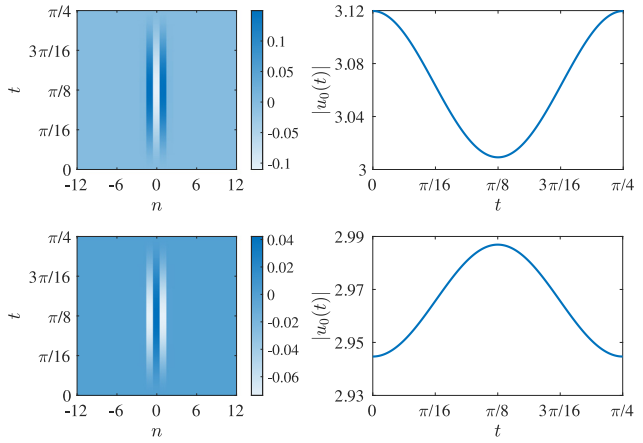

Fig. 4. Complementary numerical results associated with the dynamics presented in Fig. 3. The left and right columns present the difference of the amplitude $|u_n(t)| - |u_n(t=0)|$ and temporal evolution of $|u_0(t)|$, i.e., the amplitude of the solution at the center of the lattice, respectively. The top and bottom rows of the figure correspond to the time-periodic solutions associated with the states (a) and (f) shown in the top panel of Fig. 1 (whose spatio-temporal evolution is presented in Figs. 3(a) and (d), respectively). (For interpretation of the references to color in this figure legend, the reader is referred to the web version of this article.)

this defocusing case too. These defocusing regime instabilities manifest themselves at later times. This is due to the fact that fewer unstable eigendirections emerge in the defocusing regime, and simultaneously their growth rates are smaller compared to the ones in the focusing one. Indicatively, in Figs. 3(c) and (d), the dominant unstable eigendirection respectively corresponds to $\lambda_r \approx 1.517$ and $\lambda_r \approx 1.544$ as compared with $\lambda_r \approx 2.157$ of Figs. 3(a) and (b).

We complement the results of Fig. 3 with the panels of Fig. 4. The left and right columns of the figure demonstrate the spatio-temporal dependence of the difference of the amplitudes $|u_n(t)| - |u_n(t=0)|$ and temporal evolution of the amplitude of the central site, i.e., $|u_n(t)|$, respectively, for the cases of Figs. 3(a) (top row, focusing regime) and (b) (bottom row, defocusing regime). Recall that in this work, we were motivated by the possibility of identifying a localized in-space, time-quasiperiodic (i.e., periodic in its modulus) solution that would share some of the features of rogue waves (solutions of extreme amplitude that "appear out of nowhere and disappear without a trace") of the KM type that sits on a flat background. Our original motivation involved waveforms that would share these characteristics, designed in an "on-demand" way (as similar to a KM or Peregrine waveform) at the AC limit. The dynamics of Fig. 4, however, demonstrate that the amplitude of the oscillations of the solutions does not share the "extreme" feature of the rogue patterns but is, instead, rather "small" (compared to the size of the background), thus distinguishing between the patterns identified and the continuum (as well as integrable discrete) rogue ones. Nevertheless, the waveforms identified are novel quasiperiodic ones on a finite background that should be accessible, in principle, in optical or atomic settings where the DNLS is the suitable physical model. Importantly, also, and while the AC limit may not provide as straightforward of a path for an on-demand construction of rogue patterns, it still remains an open question whether KM breathers and Peregrine solitons on a

non-vanishing background could be identified for the physically relevant DNLS model at *finite coupling*. We discuss this central open question further in the concluding section that follows.

4. Conclusions & future challenges

In the present work we have explored the interface between two exciting recent directions, namely the study of DNLS models with an eye to applications in optical and atomic physics, and the potential of formation of rogue wave-like structures in dispersive nonlinear systems, utilizing the firm analytical handle on the latter provided by the anti-continuum limit of uncoupled lattice sites. We used a rigorous argument to showcase that relevant spatially localized but temporally quasiperiodic (periodic in the modulus) solutions should exist in such models. We illustrated a surprising continuity between the branches of associated solutions in the modulationally unstable self-focusing and the modulationally stable self-defocusing nonlinearities. This led to a snake-like bifurcation diagram featuring turning points between pairs of branches for each sign of the coupling. The defocusing solution branches were found to feature isolated (and potentially weak) instability, which, in turn, might facilitate the emergence of such states in experiments. We also examined the continuation of the relevant waveforms in the breather frequency (motivated by the corresponding continuation of the KM breather towards the Peregrine soliton), finding that while such a path can be meaningful in the focusing case, it always leads to a turning point and the absence of such solutions near $\omega_b \to 0$ for the self-defocusing realm. Finally, the dynamics of such solutions were illustrated to make the point of their controllable (according to their respective instability growth rate) persistence, most notably in the modulationally stable self-defocusing realm that may enable their potential future experimental observation. Nevertheless, as explained in detail, while our solutions are interesting novel quasiperiodic patterns on a finite background within the DNLS model, they do not share the full spectrum of rogue wave features and can thus not be characterized as ones such.

Naturally, this study raises a wide variety of additional questions and forges potential avenues for further explorations. On the one hand, it would be particularly interesting to explore the departure of the different (integrable and non-integrable) DNLS models from the continuum limit. Admittedly, this requires a different set of tools than the AC ones leveraged herein, yet it is an important question whose answer may shed light on the possibility of emergence of KM solutions to the (non-integrable) DNLS and even regarding the feasibility of their limiting Peregrine profile within the DNLS model. On the integrable systems realm, another relevant point concerns the relatively recent observation [46] regarding the exact analytical rogue waves of the *defocusing* Ablowitz–Ladik model. As these authors point out, the existence of rogue waves in the latter setting is surprising (and such waves may have also unexpected features such as a potential blowup in finite time). The potential extension of such waves in the context of the Salerno and eventually the DNLS model (in comparison with the waveforms considered herein) would also be relevant to consider. Furthermore, an interesting feature of the present considerations is that they are not dimensionally-dependent (contrary to integrability-related considerations), hence the breathers identified herein should persist to higher-dimensional cases and their properties and dynamics therein constitute another relevant vein of research. Similarly, whether quasiperiodic solutions on a finite background can be spectrally stable is yet another question of future interest. Such topics are currently under consideration and will be reported in future works.

CRediT authorship contribution statement

E.G. Charalampidis: Investigation, Methodology, Software, Writing – original draft. **G. James:** Conceptualization, Investigation, Software, Writing – original draft. **J. Cuevas-Maraver:** Conceptualization, Software, Supervision, Writing – review & editing. **D. Hennig:** Conceptualization, Methodology, Supervision, Writing – original draft. **N.I. Karachalios:** Conceptualization, Formal analysis, Supervision, Writing – review & editing. **P.G. Kevrekidis:** Conceptualization, Investigation, Methodology, Supervision, Writing – original draft.

Declaration of competing interest

The authors declare that they have no known competing financial interests or personal relationships that could have appeared to influence the work reported in this paper.

Data availability

No data was used for the research described in the article.

Acknowledgments

This work has been supported by the U.S. National Science Foundation under Grants No. DMS-2204782 (E.G.C.), and DMS-2110030 and DMS-2204702 (P.G.K.). J.C.-M. acknowledges support from the EU (FEDER program 2014–2020) through MCIN/AEI/10.13039/501100011033 (under the projects PID2020-112620GB-I00 and PID2022-143120OB-I00). EGC expresses his gratitude to D. Pelinovsky (McMaster University) and A. Scheel (University of Minnesota) for fruitful discussions.

References

[1] A.J. Sievers, S. Takeno, Phys. Rev. Lett. 61 (1988) 970–973.
[2] R.S. MacKay, S. Aubry, Nonlinearity 7 (1994) 1623–1643.
[3] S. Flach, A.V. Gorbach, Phys. Rep. 467 (2008) 1–116.
[4] S. Aubry, Physica D 216 (2006) 1–30.
[5] F. Lederer, G.I. Stegeman, D.N. Christodoulides, G. Assanto, M. Segev, Y. Silberberg, Phys. Rep. 463 (2008) 1–126.
[6] O. Morsch, M. Oberthaler, Rev. Modern Phys. 78 (2006) 179–215.
[7] P.G. Kevrekidis, The Discrete Nonlinear Schrödinger Equation, Springer-Verlag, Heidelberg, 2009.
[8] M. Jürgensen, S. Mukherjee, M.C. Rechtsman, Nature 596 (2021) 63–67.
[9] M. Jürgensen, M.C. Rechtsman, Phys. Rev. Lett. 128 (2022) 113901.
[10] M.J. Ablowitz, J.T. Cole, Physica D 440 (2022) 133440.
[11] C. Kharif, E. Pelinovsky, A. Slunyaev, Rogue Waves in the Ocean, Springer-Verlag, Berlin Heidelberg, 2009.
[12] L. Draper, Weather 21 (1966) 2–4.
[13] D.R. Solli, C. Ropers, P. Koonath, B. Jalali, Nature 450 (2007) 1054–1057.
[14] D.R. Solli, C. Ropers, B. Jalali, Phys. Rev. Lett. 101 (2008) 233902.
[15] B. Kibler, J. Fatome, C. Finot, G. Millot, F. Dias, G. Genty, N. Akhmediev, J.M. Dudley, Nat. Phys. 6 (10) (2010) 790–795.
[16] B. Kibler, J. Fatome, C. Finot, G. Millot, G. Genty, B. Wetzel, N. Akhmediev, F. Dias, J.M. Dudley, Sci. Rep. 2 (2012) 463.
[17] P.T.S. DeVore, D.R. Solli, D. Borlaug, C. Ropers, B. Jalali, J. Opt. 15 (2013) 064001.
[18] B. Frisquet, B. Kibler, P. Morin, F. Baronio, M. Conforti, G. Millot, S. Wabnitz, Sci. Rep. 6 (2016) 20785.
[19] A. Chabchoub, N.P. Hoffmann, N. Akhmediev, Phys. Rev. Lett. 106 (2011) 204502.
[20] A. Chabchoub, N. Hoffmann, M. Onorato, N. Akhmediev, Phys. Rev. X 2 (2012) 011015.
[21] A. Chabchoub, M. Fink, Phys. Rev. Lett. 112 (2014) 124101.
[22] M.L. McAllister, S. Draycott, T.A.A. Adcock, P.H. Taylor, T.S. van den Bremer, J. Fluid Mech. 860 (2019) 767–786.
[23] H. Bailung, S.K. Sharma, Y. Nakamura, Phys. Rev. Lett. 107 (2011) 255005.
[24] A. Romero-Ros, G. Katsimiga, S. Mistakidis, S. Mossman, G. Biondini, P. Schmelcher, P. Engels, P. Kevrekidis, Phys. Rev. Lett. 132 (2024) 033402.
[25] Z. Yan, J. Phys.: Conf. Ser. 400 (2012) 012084.
[26] M. Onorato, S. Residori, U. Bortolozzo, A. Montina, F.T. Arecchi, Phys. Rep. 528 (2013) 47–89.
[27] J.M. Dudley, F. Dias, M. Erkintalo, G. Genty, Nat. Photon. 8 (2014) 755–764.
[28] D. Mihalache, Rom. Rep. Phys. 69 (2017) 28.
[29] J.M. Dudley, G. Genty, A. Mussot, A. Chabchoub, F. Dias, Nat. Rev. Phys. 1 (2019) 675–689.
[30] P. Suret, R.E. Koussaifi, A. Tikan, C. Evain, S. Randoux, C. Szwaj, S. Bielawski, Nature Commun. 7 (2023) 13136.
[31] U. Teğin, P. Wang, L.V. Wang, Commun. Phys. 6 (2023) 60.
[32] D.H. Peregrine, ANZIAM J. 25 (1983) 16–43.
[33] E.A. Kuznetsov, Sov. Phys.-Dokl. 236 (1977) 575–577.
[34] Y.-C. Ma, Stud. Appl. Math. 60 (1979) 43–58.
[35] N.N. Akhmediev, V.I. Korneev, Theor. Math. Phys. 69 (1986) 1089–1093.
[36] A. Ankiewicz, N. Akhmediev, J.M. Soto-Crespo, Phys. Rev. E 82 (2010) 026602.
[37] M. Salerno, Phys. Rev. A 46 (1992) 6856–6859.
[38] C. Hoffmann, E. Charalampidis, D. Frantzeskakis, P. Kevrekidis, Phys. Lett. A 382 (2018) 3064–3070.
[39] J. Sullivan, E.G. Charalampidis, J. Cuevas-Maraver, P.G. Kevrekidis, N.I. Karachalios, Eur. Phys. J. Plus 135 (2020) 607.
[40] M. Johansson, S. Aubry, Nonlinearity 10 (1997) 1151–1178.
[41] P. Kevrekidis, M. Weinstein, Math. Comput. Simulation 62 (2003) 65–78.
[42] Wikipedia contributors, Rogue wave — Wikipedia, The Free Encyclopedia, URL https://en.wikipedia.org/wiki/Rogue_wave. (Online; Accessed 26 March 2024).
[43] Y.A. Kuznetsov, Elements of Applied Bifurcation Theory, Springer-Verlag, New York, 2023.
[44] Y.S. Kivshar, M. Peyrard, Phys. Rev. A 46 (1992) 3198–3205.
[45] N. Vakhitov, A. Kolokolov, Radiophys. Quant. Electron. 16 (1973) 783–789.
[46] Y. Ohta, J. Yang, J. Phys. A 47 (2014) 255201.